Structural Engineering and Mechanics, *Vol. 61, No. 3 (2017) 427-436*
DOI: https://doi.org/10.12989/sem.2017.61.3.427

Experimental and analytical behavior of a prestressed U-shaped girder bridge

Xun Wu* and Hui Li[a]

Department of Bridge Engineering, Tongji University, 1239 Siping Road, Shanghai, China

(Received July 8, 2015, Revised November 8, 2016, Accepted December 22, 2016)

Abstract. This paper presents an experimental and analytical investigation on the behavior of a U-shaped girder subjected to operation, cracking and ultimate loads. A full-scale destructive test was conducted on a U-shaped girder to study the cracking process, load-carrying capacity, failure mechanism and load-deformation relationships. Accordingly, the tested U-shaped girder was modeled using ANSYS and a non-linear element analysis was conducted. The investigation shows that the U-shaped girder meets the specified requirements of vertical stiffness, cracking and ultimate load capacity. Unfavorable torsional effect is tolerable during operation. However, compared with box girders, the U-shaped girder has a more transverse mechanical effect and longitudinal cracks are apt to occur in the bottom slab.

Keywords: rail transit; U-shaped girder; experiment; finite element analysis; longitudinal crack

1. Introduction

The U-shaped girder bridges have been used in the urban rail transit (URT) prestressed concrete viaducts of recent years. This section can be viewed as a conventional single-cell box girder with its top flange removed and rail transit tracks travelling between two webs (Raju and Menon 2011). Depending on the number of transit tracks between the webs, U-shaped girders are categorized into single-track and double-track types. The concept of U-shaped girder in URT was first applied on Santiago Metro Line 5 in Chile and its application shortened the schedule and reduced the construction cost by more than 20%. Since then the U-shaped girder has been popularized in projects wordwide (Dutoit *et al*. 2004). Recently, U-shaped girder was used as main girder in a tied-arch composite bridge (Wu and Gu 2014) and a U-shaped girder cable-stayed bridge (Dai and Su 2015).The U-shape bridge is one of the favorite designs possessing obvious advantages in lowing construction depth, aesthetic appearance, protection against traffic noise pollution and construction time reduction (Raju and Menon 2015, Dutoit *et al*. 2004).

However, owing to distortion, warping, transverse stress and shear lag in open thin-walled members, the structural analysis and calculation of U-shaped girders are obviously more complicated than that of closed box sections. Unfavorable warping may occur during transportation, erection and operation due to the low torsional stiffness. Hence the behavior of U-shaped girder cannot be determined simply by conventional simplified beam theory. Experimental and more advanced analytical methods are necessary to investigate the actual responses of U-shaped girder.

Extensive investigations have been carried out on thin-walled open structures in recent years. The research has included theoretical investigations (Raju and Menon 2015, Wen *et al*. 2015, Hu *et al*. 2015), analytical and numerical approaches (Puurula *et al*. 2015, Ye *et al*. 2014; Raju and Menon 2011, Dvorkin *et al*. 1989, El-Hammasi 1990) and experimental works (Galal and Yang 2009, Puurula *et al*. 2015, Chen *et al*. 2016). Wen *et al*. (2015) presented an analytical solution on the isotropic plate theory basis for analyzing concrete U-shape bridges.The mechanical performances under different vertical loads can be given in forms of mathematic expressions. In the study of Hu *et al*. (2015), the behavior of a simply supported U-shaped girder bridge was theoretical studied based on the theory of elasticity. It was showed the side beam twist has a negligible effect on the deflections and stresses of the girder. However, the theoretical methods often involve complex expression forms and are only applicable for girders with regular wall thickness and symmetric sections. Galal and Yang (2009) conducted an experimental and analytical investigation of the behavior of haunched thin-walled reinforced concrete girders and box girders. Five tests were conducted on medium-scale RC girders and box girders to study the effect of load eccentricity and the influence of bottom slabs on their ultimate load-carrying capacities, failure mechanisms and load-deformation relationships. The investigation showed that load eccentricities reduced the ultimate loads and the ductility of the girders with open sections. Chen *et al*. (2016) studied the pure torsional response of U-shaped girder. Four large U-shaped thin-walled RC beams with both ends restrained were tested. Puurula *et al*. (2015) conducted a full-scale test of a 50 year old reinforced concrete railway U-shaped bridge to investigate shear failure. The ultimate failure mechanism turned into a combination of bending, shear, torsion, and bond failures. Raju and Menon (2011) assessed

*Corresponding author, Professor
E-mail: wuxuns@126.com
[a]Ph.D. Student
E-mail: 1310222@tongji.edu.cn

ISSN: 1225-4568 (Print), 1598-6217 (Online)

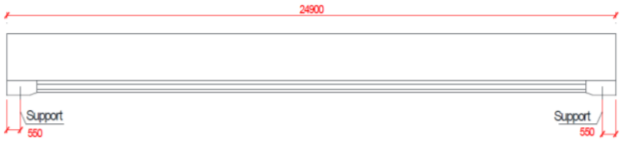

Fig. 1 Tested U-shaped girder (mm)

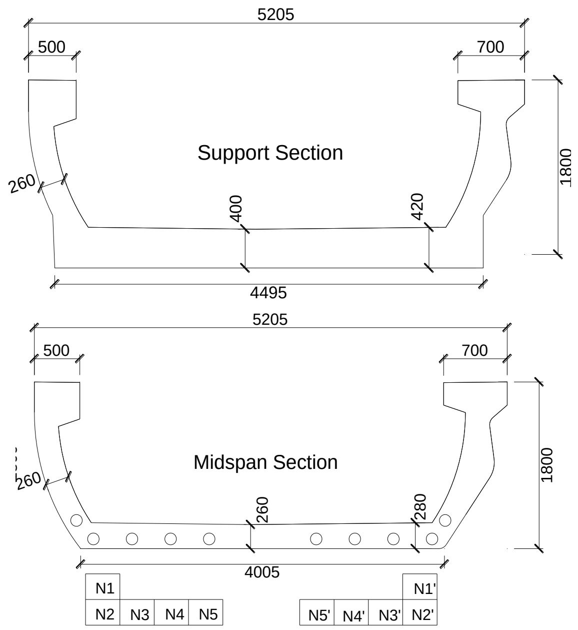

Fig. 2 Dimensions of cross-sections (mm)

the extent of error in the simplified analysis of U-shaped girders by comparing the results with a more rigorous 3D finite element analysis. The results of the 3D finite element analysis have been validated by field testing in terms of load-deflection plots.

Most previous investigations have focused on the elastic behavior of prestressed U-shaped girders. Few have considered the behavior of prestressed U-shaped girders from zero load to failure. A survey of the literature reveals that the cracking and failure behavior of prestressed U-shaped girders are still not well understood due to the lack of experimental investigation, and most design methods for box girders are not applicable to open U-shaped girders.

The objective of this paper was to obtain a better understanding of the linear and non-linear behavior of prestressed U-shaped girders. A full-scale experiment was conducted with a single- track prestressed U-shaped girder. The static mechanical performance was evaluated through the crack propagation pattern, cracking and ultimate load capacities, vertical and lateral load-deflection relationships and the strain of the steel rebars. In addition, in order to check whether finite element models can correctly capture the essential structural behavior, a non-linear finite element model was built for comparison and further analysis.

2. Bridge discription

Single-track prestressed U-shaped girders have been used in elevated sections of Nanjing Metro Line 2 Eastward in China. The span of the simply supported precast post-tensioned U-shaped girder is 25m as shown in Fig. 1.

Fig. 2 provides the detailed dimensions of the support section and midspan section in millimeters. As a simply supported beam, the U-shaped girder is 1.8 m in height, 5.205 m in width on the top and 4.005 m in width on the bottom at midspan. The thickness of the deck slab is from 0.26 m to 0.28 m and the minimal thickness of the webs is 0.26 m. Concrete C55 in Chinese code (GB 50010-2010) was used in this bridge.

Only longitudinal prestressing tendons are arranged inside the U-shaped girder as shown in Fig. 2. The tendons N1, N1', N2 and N2' are of 9 strands and the other tendons are of 7 strands. The nominal diameter of one strand is 15.2 mm. For the prestressing tendons, the ultimate strength f_{ptk} is 1860 MPa, the tensioning control stress f_p is 1860 MPa and the elasticity modulus E_s is 195 Gpa. After the prestressing tendons being tensioned, under the design dead load,the compression stress in concrete generated by prestressing tendons was about 7-8 MPa in the top flange and about 4 MPa in the bottom slab in the section at midspan.

Large numbers of ordinary reinforcments were arranged in transverse and vertical directions to improve mechanical behavior. The nominal diameters of reinforcement HPB235 in Chinese specification (standard yielding strength of 235MPa) used in the bridge are 16 mm and 25 mm.The distance between reinforcements is 14 mm. The transverse reinforcement ratio reaches 2.28% in the deck slab and the vertical reinforcement ratio is 1.14% in the two webs.

3. Experimental program

One U-shaped girder of Nanjing Metro Line 2 with a span of 25 m was tested.The experimental program was designed according to Chinese specifications for rail transit bridges, in which U-shaped girders must meet requirements of strength, cracks and stiffness. First, the actual cracking moment shall be more than 120% of the design moment; second, the actual ultimate moment shall be more than 200% of the design moment; and third, the live load deflection without impact shall be less than 1/2000 of the span. For the tested U-shaped girder, the design moment is the sum of the design dead load moment (6802 kN·m) and the design live load moment (3157 kN·m including impact).

3.1 Installation of sensors

According to preliminary calculation before test, five sections were selected as major test measurement sections including midspan section, $^1/_4$-span section, $^3/_4$-span section and two support sections. For each measured section, numerous sensors was installed including displacement meters, vibrating wire strain gauges, vibrating wire reinforcement strain meters and resistance strain gauges. The displacement meters were used to obtain the vertical and lateral deflections of the five sections. The vibrating wire strain gauges were implanted both transversely and

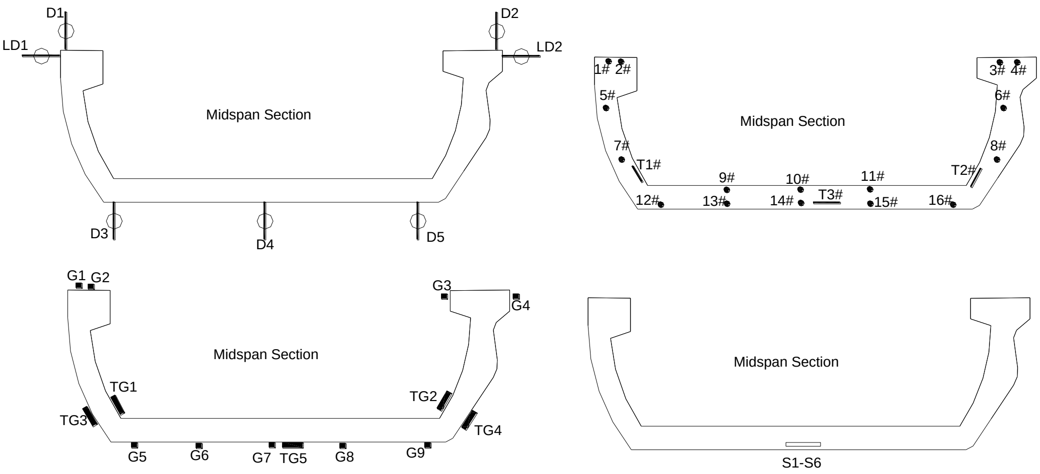

Fig. 3 Configuration of sensors in the section at midspan

longitudinally to measure the corresponding concrete strains. The vibrating wire reinforcement strain meters were located inside the deck slab of the midspan section to measure the transverse rebar strains. In addition, resistance strain gauges were applied in the five sections to measure the surface strains of the concrete and dummy resistance strain gauges were glued to concrete specimens of the same age as the actual U-shaped girder. To decrease measurement error, the measurement data was corrected to eliminate the temperature effect.The results from vibrating wire strain gauges were compared with those from resistance strain gauges to determine whether concrete cracking had occurred. There were 35 displacement meters, 64 vibrating wire strain gauges, 6 vibrating wire reinforcement strain meters and 70 resistance strain gauges in total.

In this section of the paper, the sensors arrangement of midspan section is described. Fig. 3 shows the configuration of displacement meters, vibrating wire strain gauges, resistance strain gauges and vibrating wire reinforcement strain meters in midspan section. ‘D+numbers’ and ‘LD+numbers’ refer to the vertical and lateral deflection meters, respectively. ‘T+numbers’ and ‘numbers+#’ refer to the transverse and longitudinal vibrating wire strain gauges for concrete, respectively. ‘TG+numbers’ and ‘G+numbers’ refer to the transverse and longitudinal resistance strain gauges for concrete, respectively. ‘S+numbers’ refer to the vibrating wire reinforcement strain meters for transverse rebars.

3.2 Uniaxial compressive stress-strain relation for concrete

The compression strength of tested concrete cube (150 mm×150 mm×150 mm) was 71 MPa and the elasticity modulus of concrete E_c was 42.5 GPa, both of which meet the specification for C55 according to Chinese concrete code (GB 50010-2010). For the compressed concrete in top flanges of the two webs, there is clearly a nonlinear stress-strain relationship at a high stress level. In this experiment, the measured concrete strains were transformed into stresses using the suggested uniaxial stress-strain relationship in Chinese code for the design of concrete structures (GB 50010-2010). The crushing of the top flange concrete at midspan is assumed to be the critical mark of ultimate load capacity. The suggested stress-strain relationship is shown in Eqs. (1)-(4).

$$\sigma = f_c\left[1-\left(1-\frac{\varepsilon_c}{\varepsilon_0}\right)^n\right] \tag{1}$$

$$\varepsilon_0 = 2000+5\left(f_{cu,k}-50\right) = 2105\mu\varepsilon \tag{2}$$

$$\varepsilon_u = 3300-10\left(f_{cu,k}-50\right) = 3090\mu\varepsilon \tag{3}$$

$$n = 2-\frac{1}{60}\left(f_{cu,k}-50\right) = 1.65 \tag{4}$$

Where f_c represents the uniaxial compression strength taken as 46 MPa; $f_{cu,k}$ represents the compression strength of concrete cube (150 mm×150 mm×150 mm) taken as 71 MPa; ε_c represents the measured concrete strain without shrinkage and creep; ε_0 represents the compression strain of concrete when concrete stress reaches f_c, taken as 0.002105; ε_u represents the ultimate compression strain of concrete taken as 0.00309.

3.3 Testing procedure and load cases

The standard metro train of Nanjing Metro Line 2 consists of six carriages including four motor cars and two trailers. Fig. 4 shows the standard axle weight and axle distances of the carriages. For the tested simply supported U-shaped girder with a span of 25 m, the impact factor is considered to be 1.18, so the experimental axle weight shall be 189kN.

Three critical load cases were designed and represented as LC1, LC2 and LC3. In LC1, the operation load causing maximum moment in midspan section were applied. In LC2, a cracking load case, the U-shaped girder is loaded until cracking; and in LC3, an ultimate load case, the U-shaped girder is loaded until its ultimate load capacity.

The operation load case LC1 was conducted according to the influence lines of the tested simply supported bridge.

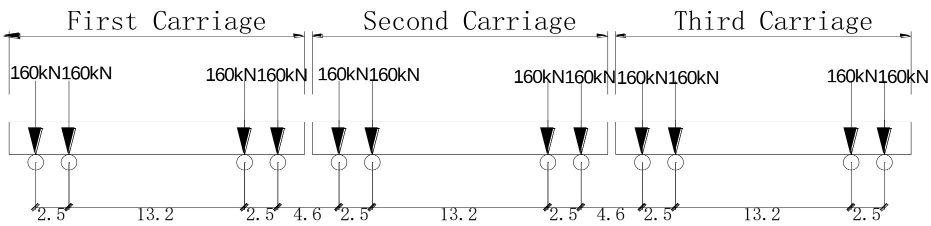

Fig. 4 Standard metro train (m)

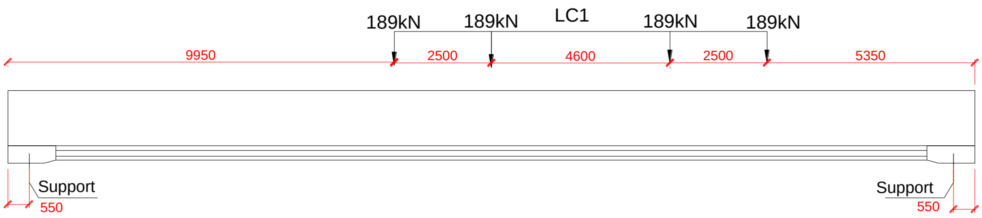

Fig. 5 Loading locations of LC1 (mm)

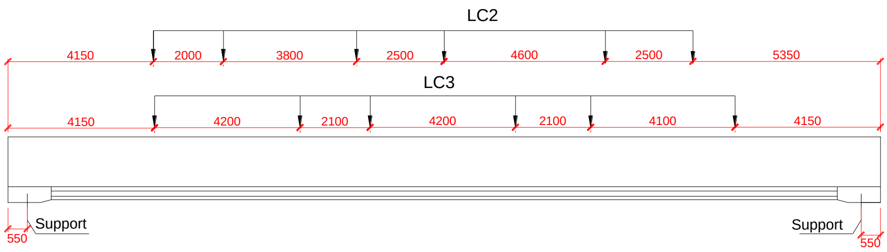

Fig. 6 Loading locations of LC2 and LC3 (mm)

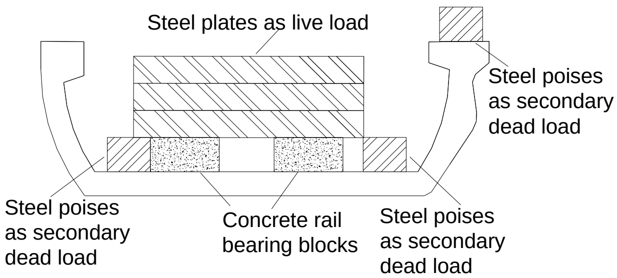

Fig. 7 Sectional view of loading

The loading location of LC1 is showed in Fig. 5. The cracking load case LC2 and the ultimate load case LC3 were designed based on LC1 and the loading locations are showed in Fig. 6.

The secondary dead load contains weights of transit facility and pavement. In the test,the secondary dead load were simulated using steel poises in three longitudinal lines, one of which was on the top flange and the other two were on the deck slab (see Fig. 7).The loading of live loads was simulated with steel plates in designed locations.

4. Test results

4.1 Specified evaluation of the U-shaped girder

Fig. 8(a) shows the operation loading stage. In LC1, the loading was applied in four steps. In the last loading step of LC1, the tested maximum live load deflection was 5.79 mm without impact load, which was less than the specified requirement for vertical stiffness (1/2000 of the span).

Fig. 8(b) shows the cracking loading stage. In LC2, 85%, 102%, 118% and 120% of the design moment were applied in four steps.No transverse cracks were observed in the loading process. However, when the loading moment reached 120% of the design moment, the first longitudinal cracks were observed in the bottom slab at $^{1}/_{4}$-span. Then 123%, 130%, 134%, 139%, 144%, 152%, 156% and 161% of the design moment were applied step by step.At the end of LC2 the first transverse crack was observed in the bottom slab at midspan. Clearly, the cracking moments almost meet the specified requirement of 1.2 times the design moment.

Fig. 8(c) shows the ultimate loading stage. In LC3, 110%, 132%, 152%, 193% and 203% of the design moment were applied in five steps. The concrete strain did not yet achieve the ultimate compressive strain when loading moment reached 203% of the design moment. Then 230%, 250% and 272% of the design moment were applied. At the end of LC3, the compressive strain of top flange in midspan reached 2173 με, which is over the limit value 2105 με. Since the loading moment had already reached a raletively high level, which was over the specified 200% of the design moment, the experiment stopped at the end of LC3 to avoid the sudden collapse of the whole structure. It was suggested that the U-girder had reached the ultimate load capacity, which was 272% of the design moment.

The vertical deflections of point D4 (see Fig. 3) during the loading process was taken to plot the total load-deflection curve in the test, as shown in Fig. 9. The moment

(a) Operation stage LC1

(b) Cracking stage LC2

(c) Ultimate stage LC3

Fig. 8 Typical loading stages

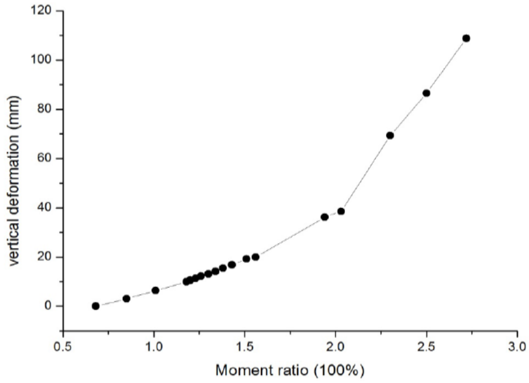

Fig. 9 Total load-deflection curve in the test

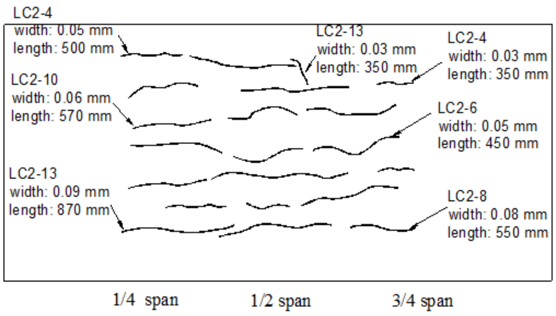

(a) Longitudinal cracks

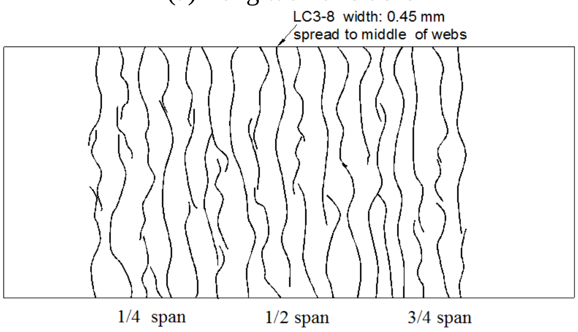

(b) Transverse cracks

Fig. 10 Crack patterns in deck slab

ratio in horizontal axis represents the ratio of the loading moment to the design moment.

It is concluded that the single-track U-shaped girder can meet the cracking, ultimate load capacity and vertical stiffness requirements. Likewise, the design of the U-shaped girder for Nanjing Metro Line 2 was proven reliable.

4.2 Crack patterns of the U-shaped girder

In LC2, when the loading moment reached 120% of the design moment, the first longitudinal cracks were observed in the deck slab at ¼-span. When the loading moment reached 161% of the design moment, the first transverse crack was observed in the deck slab at midspan. In LC3, when the loading moment reached 253% of the design moment, inclined cracks in webs were observed near the supports. Finally, when the loading moment reached 272% of the design moment, vertical cracks in webs were observed at midspan. The transverse, vertical and inclined cracks in the U-shaped girder were similar to those found in traditional concrete beams. However, due to the transverse moment and the Poisson's ratio effect, U-shaped girders are apt to crack longitudinally, which indicates the obvious transverse mechanical effect.

Fig. 10 shows the observed longitudinal and transverse crack patterns on the underside of the deck slab. The longitudinal cracks occurred first near the ¼-span section. The widths of these cracks were between 0.03 mm and 0.04 mm, and the lengths were between 0.35 m and 0.5 m. With the incremental loading, longitudinal cracks developed and coalesced. At the end of LC2, the maximum longitudinal crack width was 0.09 mm and its length was 0.87 m. As for the transverse cracks, after the first transverse crack occurred, additional transverse cracks developed rapidly. At the end of LC3, transverse cracks had spread to the middle of webs and the maximum transverse crack width was 0.45 mm.

Compared with the longitudinal cracks, the transverse cracks were longer. The longitudinal cracks occurred earlier than the transverse cracks but developed less rapidly. The longitudinal cracks and the transverse cracks rarely cross each other, which mean their interaction was not obvious. The longitudinal cracks scarcely closed once they had occurred, which was unfavourable for concrete durability. Moreover, longitudinal cracks were always located near prestressed ducts and this phenomenon could lead to stress corrosion of prestressed tendons.

4.3 Section deformation

The deformation of the U-shaped section was inferred by the deflections of measured points. Table 1 shows the vertical and lateral deflections of the midspan section at the end of each loading stage. The positive directions of deflections and a schematic diagram of section deformation are shown in Fig. 11.

At the end of LC1, the vertical deflection difference between the top and bottom was approximately 1 mm and the lateral deflection difference was within 2 mm, indicating slight torsional deformation occurred in the U-section. At the end of LC2, the vertical deflection difference between the top and bottom was over 4 mm. Finally, at the end of LC3, the vertical deflection difference between the top and bottom was over 30 mm and the lateral deflection difference was over 12 mm, indicating considerable torsional deformation occurred in the U-shaped section. It can be implied that although the torsion capacity is weak, the torsional effect on U-shaped girders is tolerable in operation and cracking stage, whereas the torsional deformation is significant in ultimate stage.

4.4 Transverse rebar stress

Located inside the deck slab of the midspan, S1-S6 (see Fig. 3) represented six vibrating wire reinforcement strain meters measuring transverse rebar strains. The measured strains were transformed into stresses with classical elasto-plastic constitutive relation of steel bars.In this section of the paper, the relationship between transverse rebar stress and loading moment is discussed. Experimental data of S3 were selected as an example.

Table 1 Deflections at the end of three loading stage (mm)

	D1	D2	D3	D4	D5	LD1	LD2	Difference*
LC1	6.6	5.58	6.78	6.83	6.21	0.59	0.99	1.25
LC2	17.46	15.20	19.24	19.97	17.94	4.26	3.13	4.77
LC3	80.40	76.01	101.51	108.83	100.17	12.33	4.85	32.82

*Difference: the maximum vertical deflection difference between the top and bottom

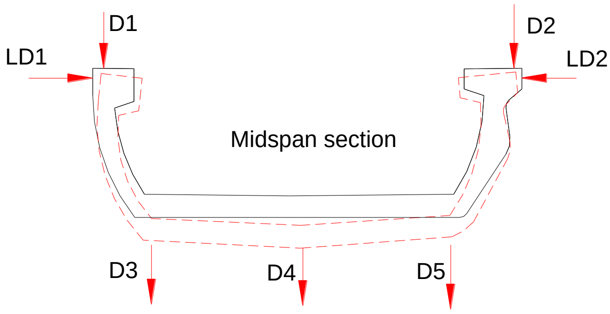

Fig. 11 Deformation of midspan section

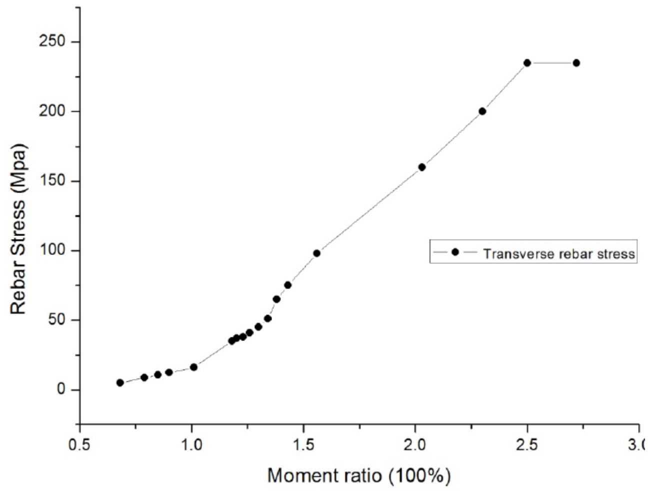

Fig. 12 Transverse rebar stress of S3

Fig. 12 shows the relationship between loading moment and transverse rebar stress in the test. In Fig. 12, the horizontal axis represents the ratio of the loading moment to the design moment and the vertical axis represents the transverse rebar stress.

The curve in Fig. 12 indicates that in operation stage LC1, the transverse rebar stress grew proportionate to the loading moment due to the well bond between concrete and rebars. In cracking stage LC2 (120% to 161% of the design moment), due to the redistribution of internal force between concrete and rebars after cracks occurred, the transverse rebar stress grew nonlinearly with the loading moment. However, in ultimate loading stage LC3 (over 161% of the design moment), an almost linear relationship between the loading moment and the transverse rebar stress was demonstrated, because the total transverse internal force was mainly undertaken by transverse rebars. In addition, the rebar stress of the six measuried points tended to be uniform during the loading procedure.

5. Numerical study

A non-linear finite element model was built for comparison and further analysis. The objective lies in two main aspects. Firstly, numerical results are compared to experimental data in terms of stress and deformation to validate the accuracy of FEM (finite element method). Secondly, the numerical results obtained from FEM can be used for other analysis, such as shear lag effect and longitudinal crack width.

5.1 Finite element analysis model

The finite element computer program ANSYS was used to conduct the numerical analysis of the tested bridge. In this study, the reinforced concrete was simulated by solid finite elements while the prestressing tendons were simulated by link elements. The geometric characteristics of the model were based on the tested U-shaped girder. The material characteristics of the model were based on material

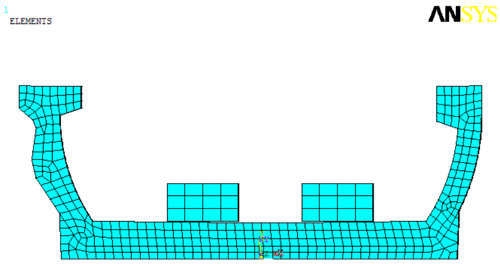

(a) Mesh generation of the support section

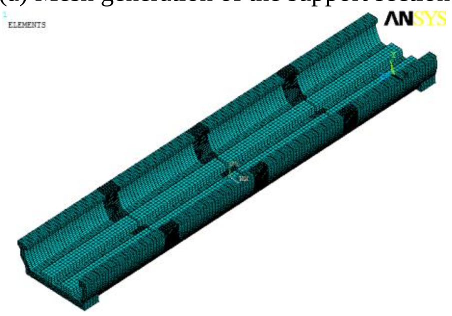

(b) Finite model

Fig. 13 Finite element analysis model of the U-shaped girder

properties test. For concrete, the compressive nonlinear constitutive relation is provided referring to Eqs. (1)-(4). The ultimate tensile strength f_t is 3.68 MPa and the elasticity modulus E_c is 42.5 GPa. The effects of concrete creep and shrinkage were not considered because these factors were eliminated from the experimental results. For steel reinforcment, classical elasto-plastic constitutive relation is adopted.The yield strength of reinforcment f_y is 235 MPa and the elasticity modulus E_s is 200 GPa.

ANSYS provides a wide variety of element types. In this study, element solid65 was used to simulate the reinforced concrete, and element link8 was used to simulate the prestressing tendons. The prestressing force was applied by defining initial strains for link8 elements and the reaction between concrete and prestressing reinforcement was simulated by coupling DOFs. Fig. 13(a) shows the mesh generation of the support section. The finite element model included 50384 solid elements and 1272 link elements.

5.2 Deflection comparison

Table 2 provides a brief comparison of tested deflections and FEM deflections at midspan at the end of each loading stage. Vertical deflection of D4 and lateral deflection of LD1 were taken as examples. According to Table 2, the theoretical vertical deflections using FEM show good agreement with the experimental results, with only a small (within 5%) error remaining. Although the relative error is large, the theoretical lateral deflections are close to the experimental results and the difference is within 2 mm.

It is found the relative error in Table 2 is always negative.This is because the material properties of concrete used in FEM was obtained by strength and elasticity modulus test of concrete specimen. Owing to the

Table 2 Comparison of tested deflections and FEM deflections at midspan (mm)

Load Case	D4			LD1		
	Tested	FEM	Relative error	Tested	FEM	Relative error
LC1	6.83	6.76	-1%	0.59	0.56	-5%
LC2	19.97	19.16	-4%	4.26	3.67	-14%
LC3	108.83	104.20	-4%	12.33	10.40	-16%

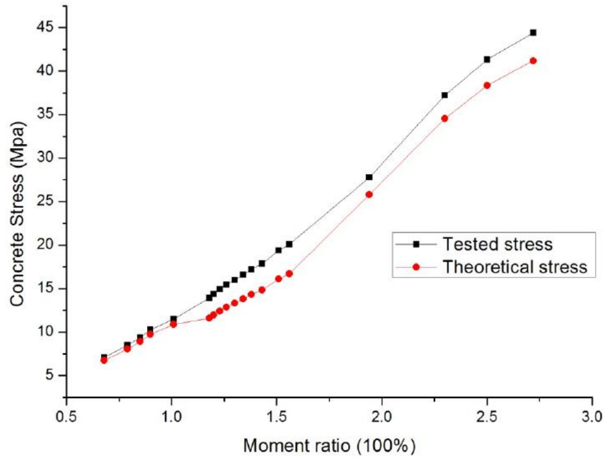

Fig. 14 Comparing the concrete stress of 3#

discreteness of concrete material property, the actual strength and elasticity modulus of the tested girder may be less than those used in finite element models. Thus the results of FEM in Table 2 are always slightly smaller than the results from the test.

5.3 Concrete stress comparison

The concrete of the top flange in midspan section had been in compression throughout the loading procedure. The comparison of stresses of point 3# (see Fig.3.) in midspan section is taken as an example. A contrast diagram of the experimental and FEM results of LC1, LC2 and LC3 is given in Fig. 14, in which the horizontal axis represents the ratio of the loading moment to the design moment and the vertical axis represents the longitudinal compressive stress of concrete. It can be concluded from Fig. 14 that the experimental and FEM results agree well, since the error is within a tolerable range. The proposed FEM was proven to be reliable and capable of effectively simulating the actual U-shaped girder.

5.4 Shear lag effect analysis

As a thin-walled open section, U-shaped girder is at obvious risk of shear lag effect, especially in the deck slab under vertical loads. To analyze the shear lag effect, the shear lag factor is defined, as expressed in Eq. (5).

$$\lambda = \frac{\sigma_r}{\sigma_0} \tag{5}$$

where λ represents the shear lag factor, σ_r represents the real longitudinal concrete stress and σ_0 represents the longitudinal concrete stress calculated by simple beam theory.

The numbers of measured longitudinal stress in test are not enough for accurate analysis of shear lag effect. Since the results of the FEM agree well with the experimental results, concrete longitudinal stress of FEM can be utilized for shear lag analysis.

Shear lag effect of $^1/_4$-span section, midspan section and $^3/_4$-span section were analyzed. For each section, forty points in the centre of the deck slab were marked, as shown in Fig. 15. Since concrete stress level in operation stage is a critical issue when bridge is designed, shear lag in operation stage is of interest. The shear lag effect at the end of LC1 was studied in detail. The shear lag factor of each marked points was calculated with Eq. (5) and the results are plotted in Fig. 16.

In midspan section, the maximum shear lag factor was about 1.54. The shear lag factor was more than 1 in the left part and less than 1 in the right part (Fig. 16). It can be explained by the bending deformation in the horizontal plane occurred in the U-shaped girder, which led to the left part in compression and the right part in tension. For the shear lag factor in LC1, the variation range of the midspan section was larger than that of the other two sections. The shear lag effect is more obvious where the longitudinal concrete stress is larger.

5.5 Longitudinal crack width prediction

The crack widths of reinforced concrete structures are directly proportional to the rebar stress and related to rebar diameters and reinforcement ratios. For longitudinal cracks affectthe service capacity and durability of U-shaped girders, a method which can calculate the longitudinal crack width is of great use. A trial approach is to calculate the longitudinal crack widths by the formula specified to calculate transverse crack widths for traditional box girders in Chinese railway bridge code (TB 10002.3-2005), as shown in Eq. (6).

$$w_f = K_1 K_2 r \frac{\sigma_s}{E_s}\left(80 + \frac{8+0.4d}{\sqrt{\mu_z}})\right) \tag{6}$$

Where w_f represents the predicted crack width in mm; r represents the ratio of the distance between the neutral axis and the tensile edge to the distance between the neutral axis and the tensile reinforcement centre; K_1 represents a factor related to rebar shapes and was taken as 0.8 in this study; μ_z represents the effective tensile reinforcement ratio; d represents the tensile reinforcement diameter and K_2 represents a factor related to loading characteristics. K_2 can be calculated by Eq. (7), but not over 1.2.

$$K_2 = 1 + \alpha \frac{M_1}{M} + 0.5\frac{M_2}{M} \tag{7}$$

Where α represents a shape parameter taken as 0.3 for ribbed rebars in this study; M_1 represents the live load moment; M_2 represents the dead load moment and M represents the total moment.

The longitudinal crack widths were predicted using the tested transverse rebar stresses and Eq. (6). Fig. 17 shows the tested and predicted longitudinal crack widths according to different stress gauges when the loading moment was 120% and 161% of the design moment. The comparison result shows that the experimental results agree with the analytical results and Eq. (6) can be used to effectively estimate the longitudinal crack width for U-shaped girders.

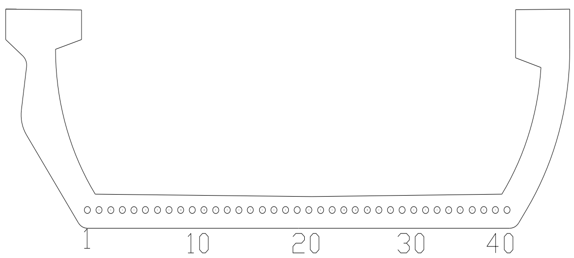

Fig. 15 Selected points for shear lag study

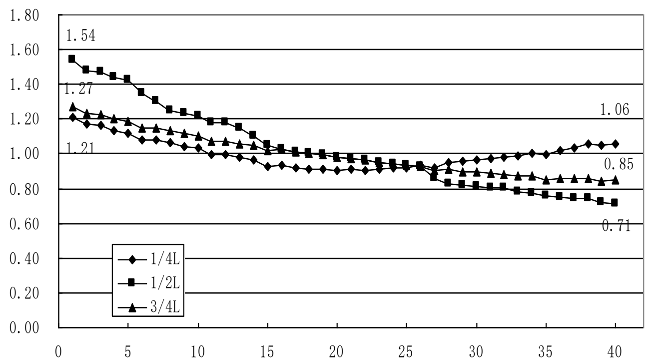

Fig. 16 Distribution of shear lag factors at the end of LC1

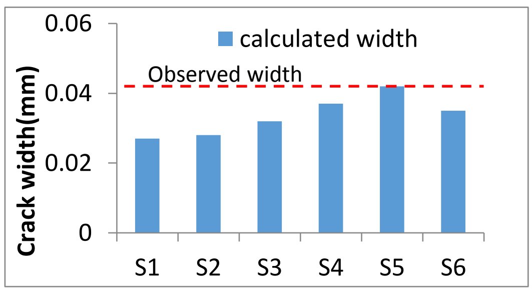

(a) 120% of the designed moment

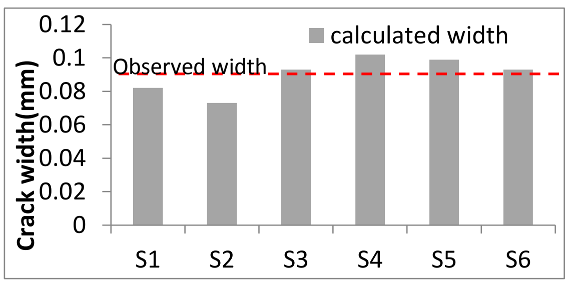

(b) 161% of the designed moment

Fig. 17 Comparison of experimental and analytical longitudinal crack widths

6. Conclusions

This paper describes a full-scale static experiment conducted on a single-track U-shaped girder. The static behavior is critically examined including deformation properties, crack patterns and failure mode. Concrete stresses, transverse rebar stress, deflections and longitudinal crack widths are measured and discussed. A finite element model was built for analysis and comparison. Given the experimental and analytical results, the following conclusions can be drawn:

- The U-shaped girder was found to meet the specified requirements of cracking, ultimate load capacity and vertical stiffness. Slight torsional deformation occurred in the operational stage and cracking stage, while serious torsional deformation occurred in the ultimate stage. In operational stage, the torsional effect of U-shaped girder is tolerable, a fact that changes the common view of the U-shaped girder.
- The longitudinal cracks in the deck slab occurred earlier than the transverse cracks. The transverse rebar stress in the bottom slab grew significantly with the loading moments. The U-shaped girder exhibits a significant transverse mechanical effect. The formula that can be used to predict longitudinal crack widths in the deck slab of U-shaped girders is proposed.
- The FEM concrete stresses and deflections show good agreement with the experimental results. The U-shaped girder has an obvious shear lag effect.The shear lag factor of section at midspan varies more severely than those of other sections. Because of the shear lag effect, the maximum concrete stress of bottom slab was almost 1.5 times the stress obtained by simple beam theory. It is suggested the shear lag effect be considered during design stage.
- For double-track U-shaped girder, the torsional effect seems to be more obvious under eccentric load. The torsional effect of eccentric load on stress and deflection in double-tracks U-shaped girder need to be further analyzed. Besides, with a wider deck slab, longitudinal cracks in deck slab are apts to occur more easily even in service stage.Therefore, to get a better understanding of transverse mechanical properties of double-tracks U-shaped girder, experimental or numerical analysis need to be conducted. It is suggested transverse prestressing tendons be applied in deck slab of double-track U-shaped girder for durability and safety of the bridge.

Acknowledgments

The authors wish to express their sincere appreciation to Nanjing Metro Co., Ltd, the Beijing Urban Construction Design Research Institute, Nanjing Metro Industrial Company and Ligao Instrument for their support during the experiment. The editors should also be recognized for their useful suggestions regarding this paper.

References

Chen, S.G., Diao, B., Guo, Q.Q., Cheng, S.H. and Ye, Y.H. (2016), “Experiments and calculation of U-shaped thin-walled RC members under pure torsion”, *Eng. Struct.*, **106**(1), 1-14.

Dai, G.L. and Su, M. (2015), “Experimental study and numerical analysis on pylon-girder rigid fixity structure of a trough girder cable-stayed bridge in high-speed railway”, *J. China Railw. Soc.*, **37**(3), 85-92. (in Chinese)

Durham, S.A., Heymsfield, E. and Schemmel, J.J. (2003), “Structural evaluation of precast concrete channel beams in bridge superstructures”, *Tran. Res. Record: J. Transp. Res. Board*, **1845**, 79-87.

Dutoit, D., Montens, S., Chuniaud, J.C. and Arnaud, P. (2004), “U-shape prestressed concrete decks for LRT/MRT viaducts”, *Proceedings of IABSE Symposium Shanghai 2004*, Shanghai, China, September.

Dvorkin, E.N., Celentano, D., Cuitiño, A. and Gioia, G. (1989), “A Vlasov beam element”, *Comput. Struct.*, **33**(1), 187-196.

El-Hammasi, S.A. (1990), “Numerical method for analysing open thin-walled structures under interaction of bending and torsion”, *Comput. Struct.*, **37**(6), 947-956.

Galal, K. and Yang, Q. (2009), “Experimental and analytical behavior of haunched thin-walled RC girders and box girders”, *Thin Wall. Struct.*, **47**(2), 202-218.

Hambly, E.C. (1991), *Bridge Deck Behaviour*, Taylor and Francis, London, UK.

Heins, C.P. (1975), *Bending And Torsional Design In Structural Members*, Lexington Books, Lexington, MA, USA.

Hu, H.S., Nie, J.G. and Wang, Y.H. (2015), “Theoretical analysis of simply supported channel girder bridges”, *Struct. Eng. Mech.*, **56**(2), 241-256.

Ministry of construction the People’s Republic of China (2010), *Code for Design on Concrete Structures. (GB 50010-2010)*, China Architecture & Building Press, Beijing, China. (In Chinese)

Ministry of railways the People’s Republic of China (2005), *Code for Design on Reinforced and Prestressed Concrete Structures of Railway Bridge and Culvert (TB 10002.3-2005)*, Chinese Railway Press, Beijing, China. (In Chinese)

Puurula, A. (2012), “Load-carrying capacity of a strengthened reinforced concrete bridge. Non-linear finite element modeling of a test to failure. Assessment of train load capacity of a two span railway trough bridge in Örnsköldsvik strengthened with bars of carbon fibre reinforced polymers (CFRP)”, Ph.D. Dissertation, Division of Structural Engineering, Luleå University of Technology, Lulea, Sweden.

Puurula, A.M., Enochsson, O., Sas, G., Blanksvärd, T., Ohlsson, U., Bernspång, L., Täljsten, B., Carolin, A., Paulsson, B. and Elfgren, L. (2015), “Assessment of the strengthening of an RC railway bridge with CFRP utilizing a full-scale failure test and finite-element analysis”, *J. Struct. Eng.*, **141**(1), SI.

Raju, V. and Menon, D. (2011), “Analysis of behaviour of U-Girder bridge decks”, *Int. J. Tran. Urban Develop.*, ACEEE, **1**(1), 34-38.

Raju, V. and Menon, D. (2015), “Longitudinal analysis of concrete U-girder bridge decks”, *Proceedings of the Institution of Civil Engineers-Bridge Engineering*, **167**(2), 99-110.

Richard, B., Epaillard, S., Cremona, C., Elfgren, L. and Adelaide, L. (2010), “Nonlinear finite element analysis of a 50 years old reinforced concrete trough bridge”, *Eng. Struct.*, **32**(12), 3899-3910.

Smith, D.A. and Hendy, C.R. (2009), “Design of the Dubai Metro light rail viaducts-substructure”, *Proceedings of the ICE-Bridge Engineering*, **162**(2), 63-74.

Vlasov, V.Z. (1961), *Thin-Walled Elastic Beams*, National Science Foundation, Washington, D.C., USA.

Wen, X., Cai, C.S., Ye, J.S. and Ma, Y. (2015), "Analytical solution on highway u-shape bridges using isotropic plate theory", *J. Civil Eng.*, KSCE, **19**(6), 1852-1864.

Wipf, T.J., Klaiber, F.W., Ingersoll, J.S. and Wood, D.L. (2006), "Field and laboratory testing of precast concrete channel bridges", *Tran. Res. Record: J. Transp. Res. Board*, **1976**, 88-94.

Wu, L.L., Nie, J.G., Lu, J.F., Fan, J.S. and Cai, C.S. (2013), "A new type of steel-concrete composite channel girder and its preliminary experimental study", *J. Constr. Steel Res*., **85**, 163-177.

Wu, X. and Gu, D. (2014), "Local stress analysis of arch foot for trough girder and arch composite bridge", *3rd International Conference on Civil, Architectural and Hydraulic Engineering (ICCAHE)*, Hangzhou, China, July.

Ye, X., Zhang, J., Ma, Y. and Han, X.D. (2014), "Study on mechanical properties of the continuous U-shaped beam", *Adv. Mater. Res.*, **889-890**, 1425-1430.

CC